



# Brain representations of affective valence and intensity in sustained pleasure and pain

Soo Ahn Lee<sup>a,b,c</sup> , Jae-Joong Lee<sup>a,1</sup>, Jisoo Han<sup>d</sup> , Myunghwan Choi<sup>a,e</sup> , Tor D. Wager<sup>f</sup>, and Choong-Wan Woo<sup>a,b,c,g,1</sup>

Edited by Allan Basbaum, University of California San Francisco, San Francisco, CA; received June 21, 2023; accepted April 18, 2024

**Pleasure and pain are two fundamental, intertwined aspects of human emotions.** Pleasurable sensations can reduce subjective feelings of pain and vice versa, and we often perceive the termination of pain as pleasant and the absence of pleasure as unpleasant. This implies the existence of brain systems that integrate them into modality-general representations of affective experiences. Here, we examined representations of affective valence and intensity in an functional MRI (fMRI) study ( $n = 58$ ) of sustained pleasure and pain. We found that the distinct subpopulations of voxels within the ventromedial and lateral prefrontal cortices, the orbitofrontal cortex, the anterior insula, and the amygdala were involved in decoding affective valence versus intensity. Affective valence and intensity predictive models showed significant decoding performance in an independent test dataset ( $n = 62$ ). These models were differentially connected to distinct large-scale brain networks—the intensity model to the ventral attention network and the valence model to the limbic and default mode networks. Overall, this study identified the brain representations of affective valence and intensity across pleasure and pain, promoting a systems-level understanding of human affective experiences.

pain and pleasure | functional MRI | predictive modeling | affective neuroscience

Pain and pleasure are two representative emotional entities of negative and positive affect (1). They interact with each other to generate a subjective interpretation of current hedonic status (2). For instance, pleasant stimuli can reduce pain, while painful stimuli can reduce pleasure. In addition, pain relief is often perceived as pleasant, and the absence of pleasure, also known as anhedonia, is common in patients with chronic pain. This implies that there exist brain systems that integrate pain and pleasure. Although painful and pleasant sensations are processed through distinct spinal and peripheral circuits (3, 4), they should ultimately be integrated into modality-general affective experiences (5, 6) in higher-level core affective brain systems (7–12). This idea has been supported by a large body of literature showing the overlap in the brain regions involved in pain and pleasure (13). Many of the overlapping brain regions are rich in opioid receptors, which play important roles in hedonic feelings and motivation (14) and the interaction between pain and pleasure (13, 15). However, most previous studies have been conducted on either pain or pleasure separately, and a direct comparison of their neural representations within the same individuals is lacking. Although some human and nonhuman primate studies (16–19) have identified a set of brain regions that respond to both positive and negative emotions, these studies have used nonpainful aversive stimuli rather than painful stimuli. A few animal studies have reported that the amygdala (20) and the anterior cingulate cortex (21) contain neurons that respond to both pain and pleasure, but these findings have been limited to specific local regions, and their generalizability to humans has not been well established.

In addition, it remains elusive how brain regions that are activated by both pain and pleasure differentially encode each type of affect. One possibility is that these brain regions represent affective valence, which ranges from negative to positive on a hedonic continuum where pain and pleasure show a marked difference (22). However, a growing number of studies have found some neural populations that also respond to both positive and negative valence, which has been referred to as the valence-general affective workspace (23), unsigned valence (24), arousal (7, 25), and salience (26, 27). We refer to this as affective intensity, which reflects the magnitudes of positive and negative feelings and is proposed as another fundamental dimension of core affect. Both affective valence (referred to here as “valence”) and affective intensity (referred to here as “intensity”) are important for decision-making and survival because they influence an organism’s approach or avoidance responses to a stimulus or situation and its perceived importance (11, 12, 28), potentially involving distinct neural populations (29). However, the brain representations of these

## Significance

Pleasure and pain, as fundamental emotional experiences, possess shared general affective dimensions such as positive vs. negative (i.e., affective valence) or weak vs. strong (i.e., affective intensity). The understanding of how these common affective dimensions across pleasure and pain are encoded in the brain carries significant clinical implications, particularly concerning pleasure-induced analgesia or anhedonia comorbid with chronic pain.

Here, we identified brain representations of affective intensity and valence shared across pleasure and pain. These two representations were not only spatially nonoverlapping with each other but also functionally connected to distinct large-scale brain networks. Our findings support the existence of the modality-general affective coding in the brain, integrating distinct sensory information of pleasure and pain into general affective experiences.

Author contributions: S.A.L. and C.-W.W. designed research; S.A.L. and C.-W.W. performed research; J.H. and M.C. contributed new reagents/analytic tools; S.A.L., J.-J.L., and C.-W.W. analyzed data; and S.A.L., J.-J.L., T.D.W., and C.-W.W. wrote the paper.

The authors declare no competing interest.

This article is a PNAS Direct Submission.

Copyright © 2024 the Author(s). Published by PNAS. This article is distributed under [Creative Commons Attribution-NonCommercial-NoDerivatives License 4.0 \(CC BY-NC-ND\)](#).

<sup>1</sup>To whom correspondence may be addressed. Email: [indaydream@skku.edu](mailto:indaydream@skku.edu) or [waniwoo@skku.edu](mailto:waniwoo@skku.edu).

This article contains supporting information online at <https://www.pnas.org/lookup/suppl/doi:10.1073/pnas.231043321/-DCSupplemental>.

Published June 10, 2024.

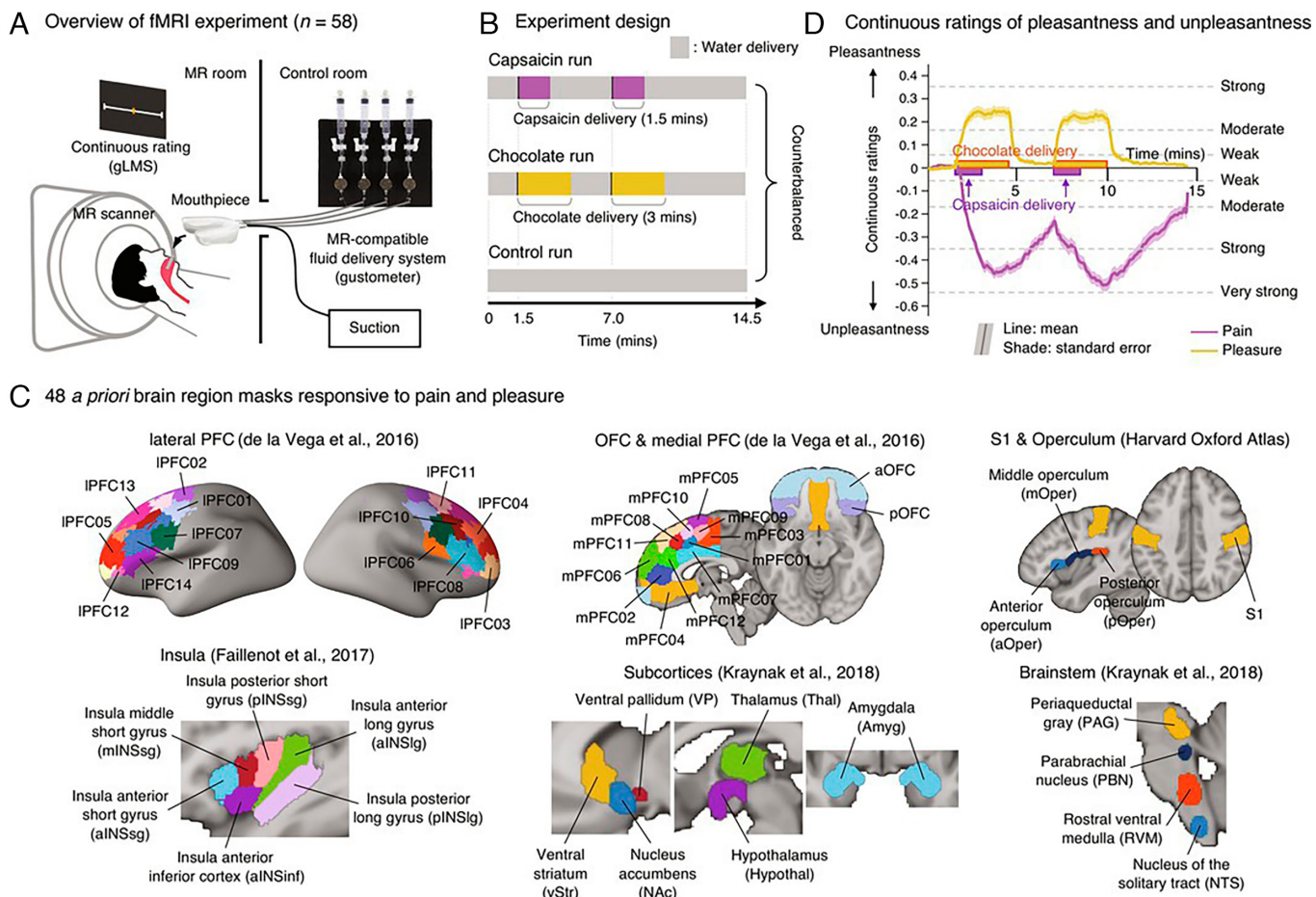


**Fig. 1.** Experimental overview and regions of interest. (A) Overview of the fMRI experiment. We delivered fluids using an MR-compatible fluid delivery system (gustometer) and removed fluids from participants' oral cavity during the experiment using a suction device. While experiencing capsaicin and chocolate fluids, participants continuously rated their subjective feelings of pleasantness and unpleasantness using the gLMS. (B) Experimental conditions included the capsaicin (pain), chocolate (pleasure), and control (neutral) conditions. Capsaicin or chocolate fluid was delivered twice in the middle of the scan, a duration of 1.5 min each for capsaicin fluid, and a duration of 3 min each for chocolate fluid. All conditions lasted 14.5 min, and their order was counterbalanced across the participants. (C) Locations of 48 *a priori* regions of interest (ROIs). The ROIs were selected based on previous literature, as provided in *SI Appendix, Fig. S1*. (D) Continuous ratings for the capsaicin and chocolate conditions ( $n = 58$ ). The solid lines indicate group average ratings (purple: pain, yellow: pleasure), and the shading indicates SEM.

general affective codes, i.e., affective valence and intensity, have yet to be identified at the systems level.

In this study, we examined the brain representations of affective valence and intensity across sustained pleasure and pain with the information mapping (30) and predictive modeling approaches (31). More specifically, our key research questions include: 1) Which brain regions contain information about pleasure and pain? Among them, which brain regions overlap? 2) Can we identify predictive models of affective valence and intensity within the overlapping brain regions? 3) Which large-scale brain networks are correlated with these predictive models? To answer these questions, we used an axiomatic approach (32, 33) to specify brain regions that contain information on pain, pleasure, and the affective dimensions shared across pain and pleasure as follows:

**Axiom 1:** Brain regions encoding information for sustained pain or pleasure must significantly predict ratings of subjective pain or pleasure.

**Axiom 2:** Of the brain regions identified in *Axiom 1*, those encoding "affective intensity" should predict both pain and pleasure ratings, irrespective of the ratings' polarity.

**Axiom 3:** Of the brain regions identified in *Axiom 1*, those encoding "affective valence" should predict both pain and pleasure ratings in relation to the ratings' directional signs.

We conducted an fMRI experiment (Study 1,  $n = 58$ ), in which participants continuously rated their subjective pleasantness and unpleasantness while experiencing sustained pain and pleasure. We induced sustained pain and pleasure by delivering capsaicin and chocolate fluids, respectively, into the participants' oral cavities via a mouthpiece (Fig. 1A). During the fMRI scans, which lasted 14.5 min and included two-times fluid deliveries, participants provided continuous ratings using a modified version of the general Labeled Magnitude Scale (gLMS) (34). Water was delivered at all other times (Fig. 1B).

We first used the multivariate pattern-based information mapping approach to identify the brain regions containing information about dynamic changes in pleasantness-unpleasantness ratings within and across individuals. Among the brain regions that showed significant decoding performance for both pain and pleasure, there were seven overlapping brain regions, including the ventromedial and lateral prefrontal cortices, the posterior orbitofrontal cortex, the ventral anterior insula, and the amygdala, which largely correspond to the neural reference space for core

affect (8). We then developed predictive models of valence and intensity using these seven overlapping brain regions to identify and compare the fine-grained brain representations of each affective dimension (23). Both the valence and intensity models showed significant prediction performance in the training and independent test datasets (Study 2,  $n = 62$ ). The important predictive features of these models included largely nonoverlapping subregions distributed across the seven brain regions. The colocalized, but distinct, brain representations of valence and intensity were correlated with distinct large-scale brain networks. The valence model was correlated with the limbic and default mode networks, whereas the intensity model was correlated with the ventral attention network.

## Results

### Identifying Brain Regions Containing Information of Sustained Pleasure and Pain.

To address the first research question ("Which brain regions contain information about pleasure and pain? Among them, which brain regions overlap?"), we identified a set of brain regions whose activation patterns are predictive of pleasantness–unpleasantness ratings during the chocolate (i.e., pleasure) or capsaicin (i.e., pain) condition. To minimize false positives, we limited our search to the 48 a priori ROIs known to respond to either pain or pleasure in the previous literature (Fig. 1C). The ROIs include brainstem and midbrain regions including the nucleus of the solitary tract, rostral ventral medulla, parabrachial nucleus, and periaqueductal gray (35), subcortical regions including the amygdala, ventral pallium, ventral striatum, nucleus accumbens, thalamus, and hypothalamus (35), insular cortex regions including the insula anterior inferior cortex, insula anterior/middle/posterior short gyri, and insula anterior/posterior long gyri (36), primary somatosensory cortex, anterior/middle/posterior operculum, anterior/posterior orbitofrontal cortices (OFCs), 12 parcellations of the medial prefrontal cortex (mPFC01-12) (37), and 14 parcellations of the lateral prefrontal cortex (IPFC01-14) (37). *SI Appendix*, Fig. S1, provides the list of previous studies that reported these ROIs' responses to pain or pleasure stimuli and alternative nomenclature of the medial prefrontal regions.

For each of these ROIs, we trained fMRI pattern-based models to predict pleasantness–unpleasantness ratings for the pain or pleasure condition separately. Fig. 1D shows the overall patterns of pleasantness–unpleasantness ratings for the capsaicin and chocolate conditions, which served as the outcome variable in this pattern-based information mapping. The rating patterns clearly showed varying magnitudes of pleasantness and unpleasantness induced by dual administrations of capsaicin and chocolate fluids, which is an important design feature to improve the specificity of predictive models. The individual behavioral ratings fluctuated across moderate-to-strong levels for capsaicin and chocolate deliveries (*SI Appendix*, Fig. S2). Overall pain intensity ratings collected after the capsaicin conditions also reached moderate to strong levels, suggesting that the capsaicin stimuli effectively induced pain in all participants (*SI Appendix*, Fig. S3).

We provide the details of the predictive modeling in *Materials and Methods* and *SI Appendix*, Fig. S4, but in brief, we used beta estimates of 34 time-bins from a GLM of fMRI data (i.e., 25 s per time-bin) to enhance the signal-to-noise ratio and remove nuisance effects. We applied principal component regression (PCR) on the capsaicin and control condition data to develop pain models and on the chocolate and control condition data to develop pleasure models to predict rating variability within and across individuals. To account for the different numbers of voxels in each ROI, we

used the same number of principal components (13 PCs) across ROIs (for details of how we selected the number of PC, see *SI Appendix, Materials and Methods*). We calculated model performance with the averaged within-individual correlation between predicted and actual ratings using leave-one-subject-out cross-validation (LOSO-CV).

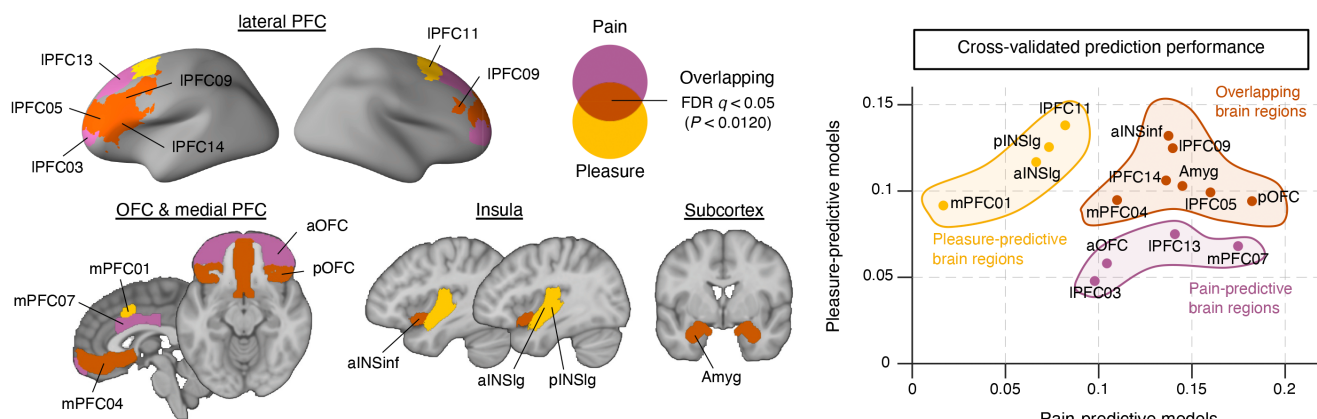
Among the 48 ROIs, seven regions showed significant decoding performance for both pain and pleasure (Fig. 2A). These include the amygdala, the insula anterior inferior cortex (which is also called ventral anterior insula; below, we added alternative region names in the parenthesis), mPFC04 (ventromedial PFC), the posterior OFC, IPFC05, IPFC09, and IPFC14 (ventro- to dorso-lateral PFC). Their mean within-individual correlations between the actual and predicted ratings were  $r = 0.11$  to  $0.18$ , mean within-individual mean squared error (mse) = 0.052 to 0.054,  $P = 0.00001$  to  $0.0045$  for predicting pain, and mean  $r = 0.09$  to  $0.13$ , mean mse = 0.021 to 0.022,  $P = 0.0005$  to 0.0105 for predicting pleasure. These were significant after the correction for multiple comparisons with false discovery rate (FDR)  $q < 0.05$ , bootstrap test, two-tailed. Many of these regions are among the brain structures that have been implicated in the common neurobiology of pain and pleasure (13) and substantially overlap with the hypothetical neural reference space of core affect (i.e., "affective workspace") (8). The brain regions important only for the prediction of pain included the anterior OFC, mPFC07 (midcingulate cortex), IPFC03 (frontal pole), and IPFC13 (presupplementary motor area). The brain regions important only for the prediction of pleasure included the insula anterior and posterior long gyri, mPFC01 (a dorsal part of the midcingulate cortex), and IPFC11 (supplementary motor area). The brainstem regions showed poor prediction performance, which could be related to their low temporal signal-to-ratio (*SI Appendix*, Fig. S5). Decoding performance was not significantly associated with the within-individual variability of pleasantness–unpleasantness ratings (*SI Appendix*, Figs. S6 and S7), the variances explained by the same number of PCs (i.e., 13 PCs; *SI Appendix*, Fig. S8A, see also *SI Appendix, Discussion*), and the number of voxels within each ROI (*SI Appendix*, Fig. S8B). For decoding between-individual variability of behavioral ratings, brain regions associated with either pain or pleasure exhibited performances that, while not statistically significant, outperformed other brain regions (*SI Appendix*, Fig. S9).

We conducted two additional analyses to examine the robustness of these findings. First, we conducted a searchlight analysis (30), in which we trained a PCR model using the same method as we did in the ROI-level modeling for each searchlight (for details, see *SI Appendix, Materials and Methods*). We provided a brain map with the explained variances with 13 PCs across searchlights and their relationship with prediction performance in *SI Appendix*, Fig. S10. With LOSO-CV, we identified a set of voxels that showed significant predictions for both pleasure and pain. Their spatial locations largely overlapped with the seven ROIs that were predictive of both pain and pleasure (Fig. 2B; see also *SI Appendix*, Fig. S11, for the same level of thresholding as Fig. 2A). Second, we tested different PC numbers (or different explained variance) for the PCR modeling, and the results showed similar patterns across PC numbers (*SI Appendix*, Figs. S12 and S13 and *Materials and Methods*). Overall, these results showed that our findings were robust across different modeling choices and methods.

### Parsing Affective Valence and Intensity within the Overlapping Brain Regions.

To address the second research question ("Can we identify predictive models of affective valence and intensity within the overlapping brain regions?"), we developed predictive models of

### A Brain regions predictive of ratings for pain and pleasure conditions



### B Searchlight analysis results showing brain regions predictive of ratings for pain and pleasure conditions

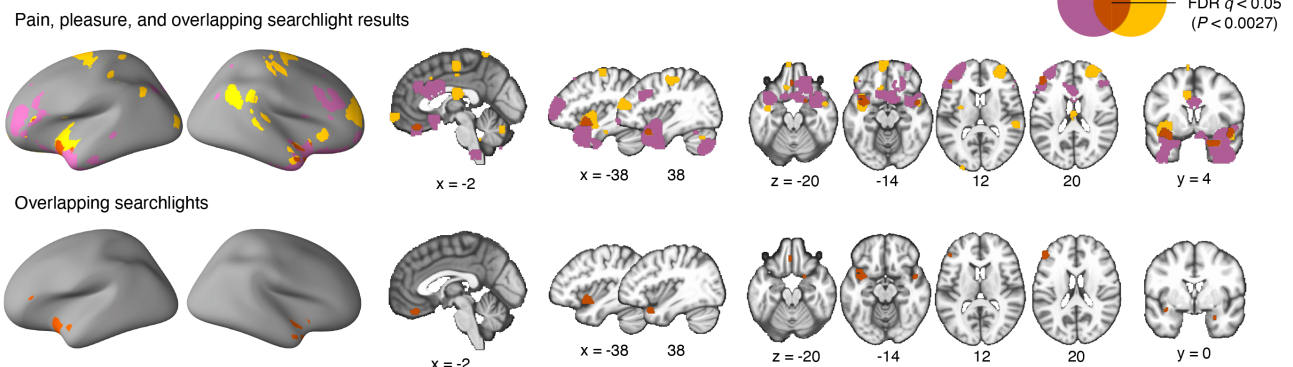


**Fig. 2.** Information mapping results. (A) *Left:* Brain regions that showed significant prediction performances ( $FDR q < 0.05$ ) at predicting the pleasantness–unpleasantness ratings for the pain and pleasure conditions (purple: pain-predictive; yellow: pleasure-predictive; vermillion: overlapping). *Right:* A scatter plot showing the cross-validated prediction performances. alNSinf, insula anterior inferior cortex; alNSlg, insula anterior long gyrus; pINSlg, insula posterior long gyrus; Amyg, amygdala; aOFC, anterior orbitofrontal cortex; pOFC, posterior orbitofrontal cortex; IPFC, lateral prefrontal cortex; mPFC, medial prefrontal cortex. (B) *Top:* Searchlight voxels that showed significant prediction performances ( $FDR q < 0.05$ ). *Bottom:* Overlapping searchlight voxels.

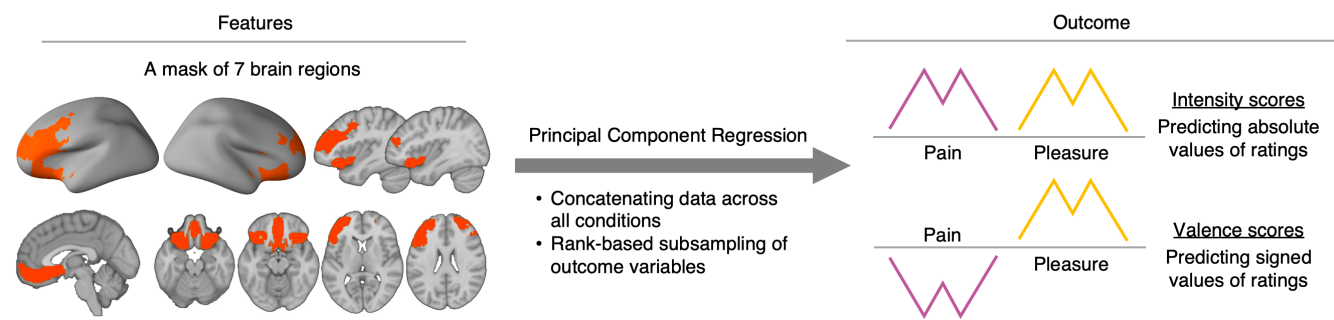
intensity and valence, which we hypothesized as two fundamental affective dimensions shared across pain and pleasure (Fig. 3*A*). We defined the absolute value of pleasantness or unpleasantness rating as an intensity score and the raw signed value of pleasantness (i.e., positive) or unpleasantness (i.e., negative) rating as a valence score. We developed PCR models to predict the intensity or valence scores using the combined data of the capsaicin, chocolate, and control conditions. We used all voxels across the seven overlapping brain regions for training the intensity and valence models because a multiple region-based model can yield better prediction performance than single region-based models by capturing information distributed across multiple brain systems (31) (for completeness, we also provided region-level intensity and valence modeling results in *SI Appendix, Tables S1 and S2*). Since the overall unpleasantness ratings induced by capsaicin were higher than the overall pleasantness ratings induced by chocolate, we matched the distribution of unpleasantness and pleasantness ratings before prediction by subsampling data and transforming the scores into ranks ( $\pm 1$  to  $\pm 10$ ; please see *SI Appendix, Materials and Methods*). The outcomes of this subsampling procedure on data selection are detailed in *SI Appendix, Fig. S14*. We tested the resulting models on the independent test dataset (Study 2) to examine their generalizability.

The results showed that both intensity and valence models showed significant prediction performance (Fig. 3*B*) in the training and independent test datasets. The leave-one-subject-out cross-validated model performance in the training dataset was as follows: For the

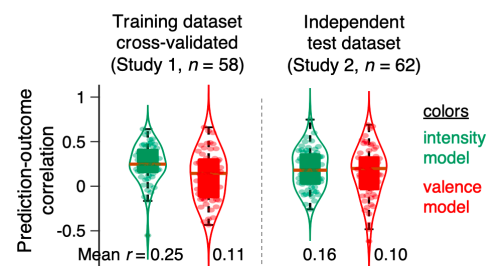
intensity model, the mean within-individual correlation between actual and predicted ratings was  $r = 0.25$ ,  $P = 2.22 \times 10^{-16}$ , bootstrap test, two-tailed, mean mse = 13.061, and for the valence model,  $r = 0.11$ ,  $P = 0.0017$ , mean mse = 23.860. The models were also predictive of each condition separately (intensity model: for the capsaicin condition, mean  $r = 0.31$ ,  $P = 4.64 \times 10^{-8}$ , mean mse = 19.958, for the chocolate condition, mean  $r = 0.23$ ,  $P = 3.53 \times 10^{-8}$ , mean mse = 14.859; valence model: for the capsaicin condition, mean  $r = 0.12$ ,  $P = 0.0235$ , mean mse = 35.740, for the chocolate condition, mean  $r = 0.08$ ,  $P = 0.0322$ , mean mse = 27.996), suggesting that these models are sensitive to both conditions. When we tested the models in the independent test dataset (Study 2), the intensity and valence models also showed significant prediction: For the intensity model, mean  $r = 0.16$ ,  $P = 3.82 \times 10^{-9}$ , mean mse = 7.198; for the valence model, mean  $r = 0.10$ ,  $P = 0.0053$ , mean mse = 7.908. Both models' pattern expression values (*Materials and Methods*) showed fluctuations in the same direction with the hypothesized trajectories in the training (Fig. 3*C*) and independent test datasets (*SI Appendix, Fig. S15*).

Although we used ranks instead of original ratings to reduce any potential biases in the models due to different ranges of ratings for the pain and pleasure conditions, we did additional training with the original ratings to examine whether rank-based prediction influenced the model performance. The results showed comparable model performance, mean  $r = 0.27$ ,  $P = 2.22 \times 10^{-16}$ , mean mse = 0.0395 for the intensity model, and mean  $r = 0.11$ ,

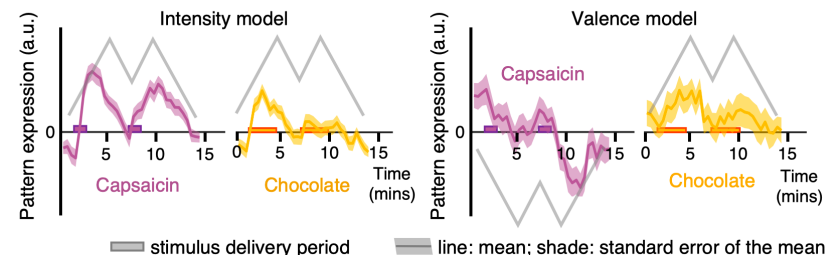
## A Analysis overview



## B Model performance



## C Pattern expression values with leave-one-subject-out cross-validation



## D Thresholded predictive maps ( $FDR q < 0.05$ )

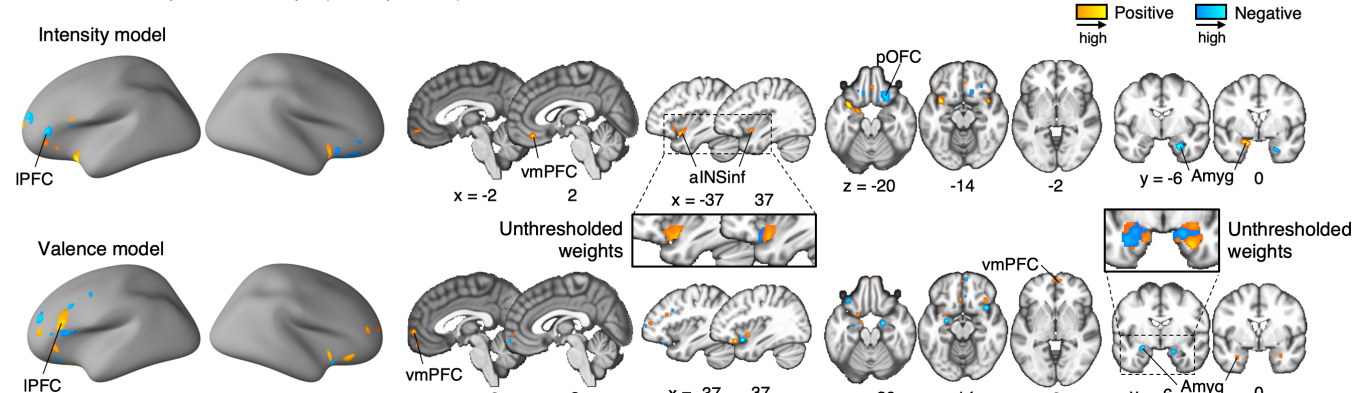


**Fig. 3.** Prediction modeling of affective intensity and valence. (A) Overview of the predictive modeling analysis. Here, we used data from the seven brain regions identified in the previous analysis. The outcome variable was either affective intensity, which was defined as the absolute values of pleasantness-unpleasantness ratings, or affective valence, which was defined as the raw signed values of the ratings. We conducted the rank-based subsampling based on the outcome variables to minimize the potential bias due to the greater rating magnitude for the capsaicin condition compared to the chocolate condition (for details, see *SI Appendix, Materials and Methods*). We applied PCR on the concatenated data across all conditions. (B) Model performance. The violin plots show the distribution of within-individual prediction-outcome correlations in the training dataset (with LOSO-CV) and the independent test dataset (green: intensity model, red: valence model). (C) The time course of pattern expression values of each model, which were calculated using LOSO-CV. The solid line represents the group average, and the shading represents the SEM (purple: capsaicin, yellow: chocolate). The boxes on the time axes indicate the fluid delivery period. (D) Predictive weight maps thresholded with  $FDR q < 0.05$  based on bootstrap tests (10,000 iterations). Insets show the unthresholded weights for ROIs.

$P = 7.62 \times 10^{-4}$ , mean mse = 0.0651 for the valence model (*SI Appendix, Fig. S16A*), suggesting that the rank-based prediction did not have a substantial impact on the model performance. We also examined whether using all 48 ROIs for the prediction could have a meaningful effect on the model performance. The models with 48 ROIs also showed comparable model performance compared to the seven ROI-based models, mean  $r = 0.25$ ,  $P < 2.22 \times 10^{-16}$ , mean mse = 13.225 for the intensity model, and mean  $r = 0.09$ ,  $P = 0.0232$ , mean mse = 24.522 for the valence model (*SI Appendix, Fig. S16B*), suggesting that the seven brain regions are sufficient to predict the affective intensity and valence.

To examine the spatial specificity of the seven ROI-based results, we conducted four additional analyses. First, we trained the intensity and valence models using the voxels within the nonoverlapping 41 ROIs. Results showed significant prediction for affective

intensity, mean  $r = 0.24$ ,  $P < 2.22 \times 10^{-16}$ , mean mse = 13.206, but a nonsignificant result for affective valence, mean  $r = 0.07$ ,  $P = 0.0869$ , mean mse = 24.523. Second, we used the voxels outside of the 48 ROIs (*SI Appendix, Fig. S17*) for training intensity and valence models. We excluded the visual cortex because the continuous rating procedure can induce an activation pattern in the visual cortex correlated to pain and pleasure experiences. Results showed significant but substantially lower prediction performance for affective intensity compared to the original results (mean  $r = 0.14$ ,  $P = 1.12 \times 10^{-6}$ , bootstrap test, two-tailed, mean mse = 13.477), and the prediction performance for affective valence was nonsignificant (mean  $r = 0.06$ ,  $P = 0.1891$ , mean mse = 24.259). Third, even when we combined the other four pain-predictive and four pleasure-predictive ROIs, consistent voxels across the seven ROIs significantly contributed to the intensity prediction (*SI Appendix, Figs. S18 and S19*).

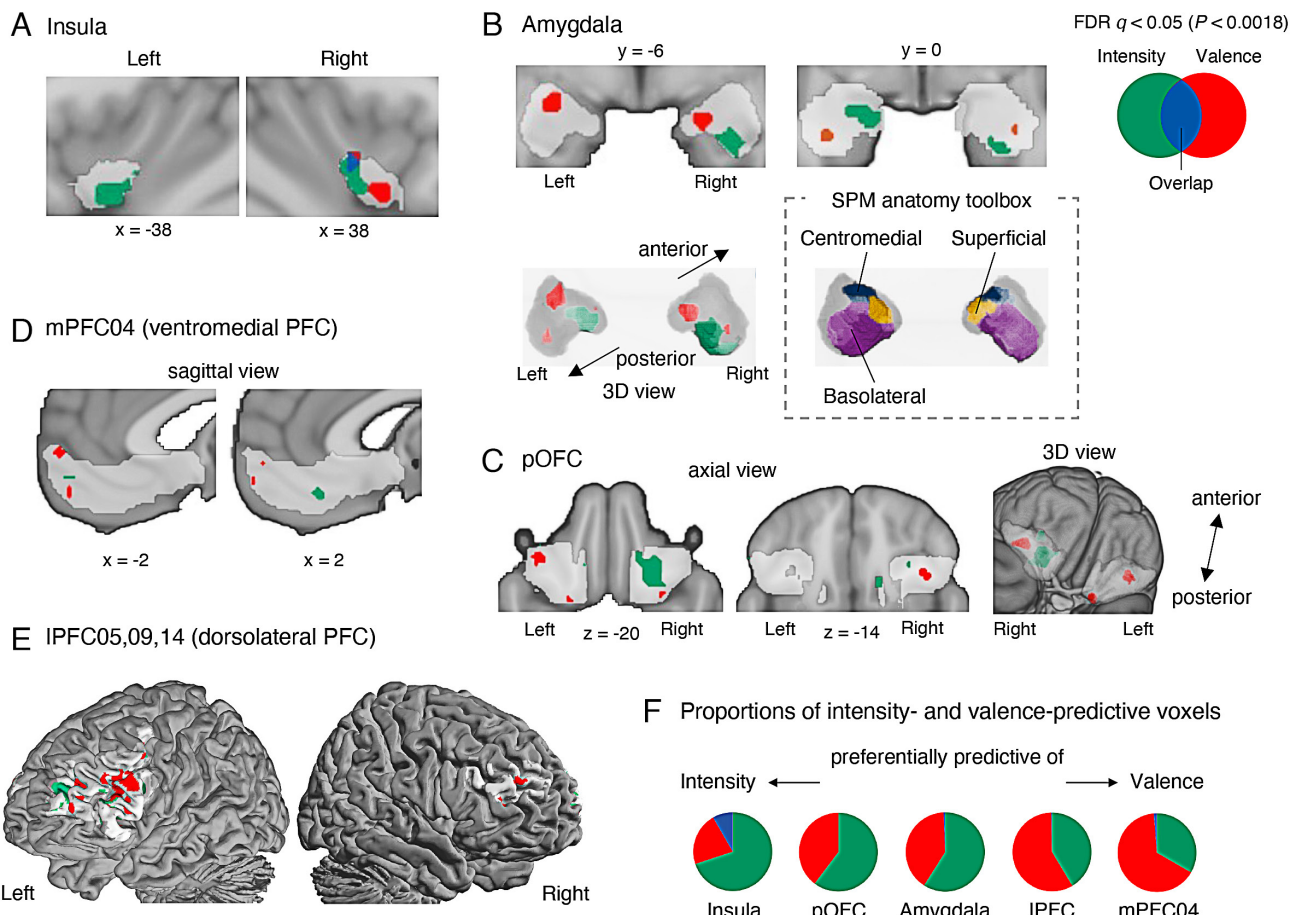


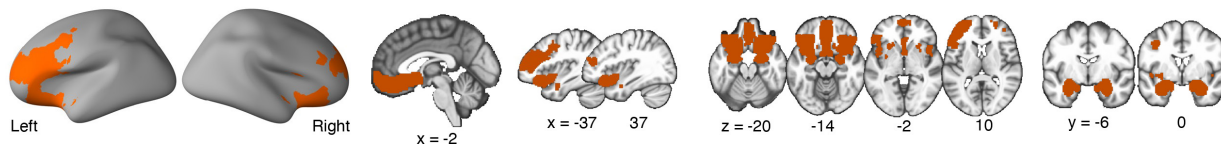
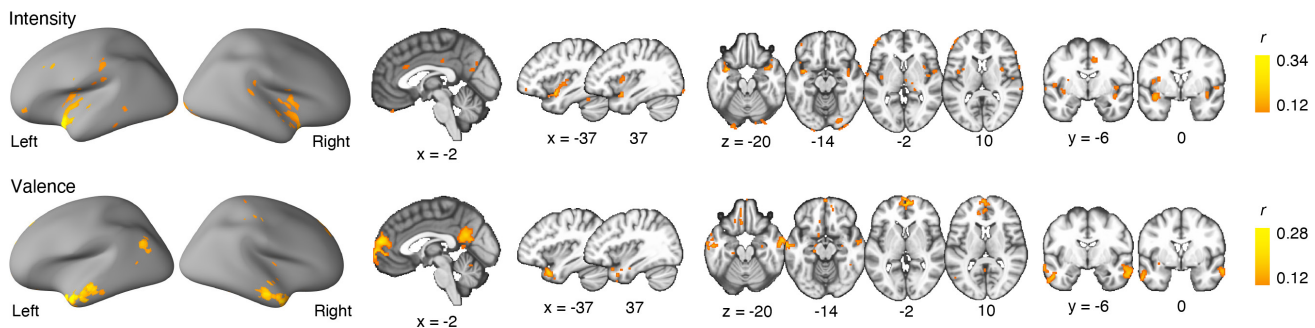
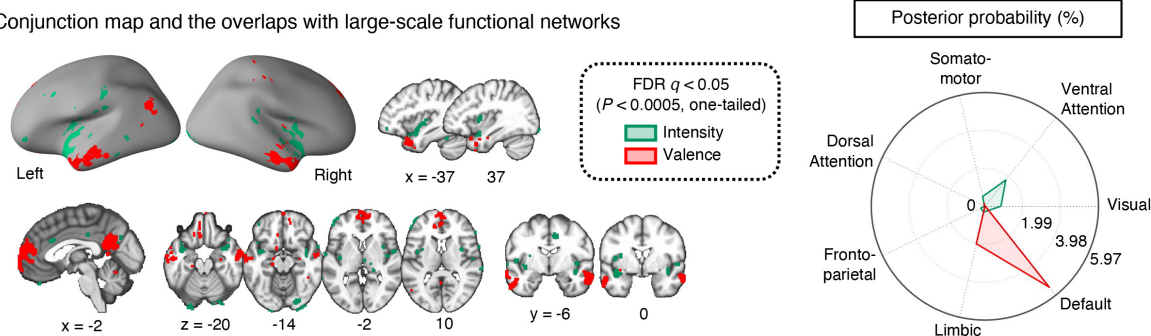
**Fig. 4.** Significant voxels of the intensity and valence models. (A–E) To examine whether the significant voxels of the two models are overlapping or not, we examined the exact locations of the significant voxels ( $FDR q < 0.05$ ) by visualizing them with different colors—green for the intensity model, red for the valence model, and blue for the overlapping voxels. Each section shows each ROI: (A) insula, (B) amygdala, (C) posterior OFC (pOFC), (D) mPFC04 (ventromedial PFC), and (E) IPFC05, 09, and 14 (dorsolateral PFC). (F) The pie charts show the proportions of significant voxels for the intensity model only (green), the valence model only (red), or both models (blue).

Fourth, a binary classification model between the capsaicin vs. chocolate conditions based on the seven ROIs, instead of predicting affective valence scores, also showed significant accuracy (accuracy = 64%,  $P = 0.0479$ , forced-choice, binomial test, two-tailed) and similar spatial patterns of model weights with the original valence model (SI Appendix, Fig. S20). Overall, these results suggest that the seven overlapping regions are crucial and showed better prediction performances for the intensity and valence prediction compared to other regions.

We compared the important voxels between the intensity and valence models based on the thresholded results at  $FDR q < 0.05$ , two-tailed, from bootstrap tests with 10,000 iterations (for the unthresholded maps, see SI Appendix, Fig. S21). The intensity and valence maps showed largely nonoverlapping spatial patterns of predictive weights (Figs. 3D and 4), suggesting that distinct subpopulations of voxels within the seven brain regions are important for decoding affective valence versus intensity information. For example, there was a cluster of intensity-predictive voxels in the bilateral ventral anterior insula (Fig. 4A), which has been known as the primary taste cortex (38) and encoding the salience of visceral sensation (38–40), but there was also a cluster of valence-predictive voxels in the right ventral anterior insula, mostly nonoverlapping with the intensity-predictive voxels (Fig. 4A). Also in the amygdala, the intensity-predictive voxels were mainly located in the ventral part of the right basolateral amygdala with negative weights and in the dorsal part of the left basolateral amygdala with positive weights (Figs. 3D and 4B). In contrast, the valence-predictive

voxels were mainly located in the left centromedial and the right superficial amygdala with negative weights. These results are consistent with previous studies that the basolateral amygdala contains a population of neurons encoding valence-general salience (20, 25), whereas the centromedial and superficial amygdala regions are important for processing negative valence (41–43). The posterior OFC contained intensity-predictive voxels mostly in the right medial part, while valence-predictive voxels in the lateral part (Fig. 4C). This is also supported by the previous finding that the medial part of this region, as a secondary gustatory cortex (38), encodes magnitude information of value (27). For the ventromedial PFC, the intensity-predictive voxels were located in the ventral part, whereas the valence-predictive voxels were located in the dorsal part (Fig. 4D), and for the dorsolateral PFC, the predictive weights of the two models were also largely nonoverlapping (Fig. 4E). In sum, these results suggest that the affective intensity and valence are represented by distinct subpopulations of voxels within the seven brain regions. However, the overall distribution of intensity- vs. valence-predictive voxels across brain regions suggests that the insula is preferentially predictive of intensity, while the ventromedial PFC is preferentially predictive of valence (Fig. 4F). To see the relative importance of all voxels for the intensity versus valence models, see SI Appendix, Fig. S21E.

**Distinct Functional Brain Networks for the Affective Intensity and Valence.** To situate the locally distinct brain representations of affective intensity and valence in the context of the global

**A** Masks of 7 overlapping brain regions as seed regions**B** Thresholded functional connectivity of the affective intensity and valence models ( $FDR \ q < 0.05$ , one-tailed)**C** Conjunction map and the overlaps with large-scale functional networks

**Fig. 5.** Functional connectivity maps for the intensity and valence models. (A) Masks of the seven overlapping brain regions as seeds. (B) Thresholded functional connectivity patterns using the pattern expression values of intensity and valence models as seeds ( $FDR \ q < 0.05$ , one-sample  $t$  test, one-tailed). The functional connectivity was calculated using the control condition data with LOSO-CV. Here, we tested the unidirectional hypothesis (i.e., focusing only on positive correlations) because the negative correlations were difficult to interpret. In addition, we excluded the brain coverage of the predictive models to focus on their relationship with other brain regions. (C) Left: Conjunction maps indicating results of the different models (green: intensity model; red: valence model). Right: A radar plot showing the posterior probability of the significant voxels within each large-scale functional network given the total number of voxels within each network.

functional brain networks (44) (*SI Appendix*, Fig. S22), we addressed the last research question (“Which large-scale brain networks are correlated with these predictive maps?”). To this end, we extracted the pattern expression values of intensity and valence models from the control condition data using the cross-validated predictive weights (45, 46). Using these pattern expression values as seeds, we obtained a whole-brain functional connectivity map for each individual by calculating Pearson correlations between the seeds and voxel-wise activity time series. We removed the seed regions (i.e., the mask of seven brain regions; Fig. 5A) from the resulting maps to help interpretation. Then, we visualized the voxels with significant positive connectivity across participants ( $FDR \ q < 0.05$ , one-sample  $t$  test, one-tailed) in Fig. 5 B and C. Here, we focused only on positive correlations because the negative correlations were difficult to interpret, but for completeness, we also provide the maps with both positive and negative correlations in *SI Appendix*, Fig. S23.

The results showed that the predictive maps of intensity and valence were correlated with distinct large-scale brain networks. As shown in Fig. 5B, the intensity model showed significant correlations in the insula and the anterior midcingulate cortex, the key regions of the ventral attention (or salience) network (39, 40), which is an aggregation of salience and cingula-opercular networks. The valence model showed significant correlations in the

ventromedial PFC and the posterior cingulate cortex, the key regions of the default mode network. In addition, there were also multiple significant voxels in the OFC and the superior temporal gyrus, which are a part of the limbic network (28). To verify the consistency of these results, we conducted two additional analyses. First, we obtained the conventional seed-based functional connectivity by using significant ( $FDR \ q < 0.05$ , two-tailed, from bootstrap tests with 10,000 iterations) positive predictive weights from the intensity and valence models as a seed mask (*SI Appendix*, Fig. S24). Second, we obtained the same functional connectivity with the pattern expressions of the intensity and valence, based on the control condition data of the Study 2 dataset (*SI Appendix*, Figs. S25 and S26). Results from these two analyses were largely consistent with the pattern expression-based functional connectivity results (Fig. 5).

## Discussion

The current study investigated the brain representations of affective valence and intensity in sustained pleasure and pain. We first identified brain regions that contained information about pleasure and pain. The brain regions included the ventromedial and lateral PFCs, the posterior OFC, the ventral anterior insula, and the amygdala. We then developed predictive models of affective intensity and

valence with these brain regions, which demonstrated significant prediction performance in both training and independent test datasets. The intensity and valence models were dissociable in their fine-grained spatial patterns of thresholded weights and were associated with the two separate large-scale functional brain networks—the ventral attention network for the intensity information vs. the limbic and default mode networks for the valence information. Overall, these results provided neuroimaging evidence of how the brain encodes pleasure and pain based on the general affective dimensions of valence and intensity.

First, our findings support the existence of overlapping brain regions that contain information for both pleasure and pain. Although the relationship between pleasure and pain has been a topic of interest for a long time (1, 13, 47), it still remains unclear in which brain regions pleasure and pain are integrated and connected. Previous studies have identified some brain regions commonly activated by pleasure and pain (13), but most of the studies examined pleasure and pain separately and did not directly compare their brain representations. Our study aimed to fill this gap by inducing both sustained pleasure and pain in each individual and identifying brain regions predictive of ratings for both conditions, by using the axiomatic approach. Using a multivariate pattern-based information mapping approach, we identified seven brain regions for pleasure and pain, including the ventromedial and lateral PFCs, posterior OFC, ventral anterior insula, and amygdala. These regions were among the brain regions that have been implicated in the pleasure–pain interaction (48–50) and the affective workspace in the brain (8). Although the stringent nature of our axiomatic approach may miss the other brain regions that encode pain or pleasure information, its rigor allowed us to identify the brain representations of complex behaviors that are susceptible to confounds, as highlighted in previous studies (32, 33).

Second, our results suggest that the two core dimensions of affective experience—*affective intensity* and *valence*—are encoded in these overlapping brain regions. We were able to develop predictive models of affective intensity and valence based on the multivariate patterns of the brain regions' activity, and the predictive models were generalizable across training and independent test datasets. These results are in line with the previous meta-analysis that there exist both valence-specific and valence-general brain regions (23). To further validate our findings, it would be interesting to explore whether the predictive models we developed are responsive to pharmacological or contextual manipulation (49, 51–54). Such investigations could have significant implications for clinical applications and represent a promising direction for future research. In addition, it is important to consider that other factors might contribute to the shared affective dimensions across sustained pain and pleasure, including salience, cognitive appraisal, and action tendencies. While it is inherently challenging to disentangle these effects, our models present an opportunity for future studies to further characterize and understand what these models represent. This ongoing investigation will enhance our understanding of the complex interplay between these various elements in shaping our affective experiences.

Third, through detailed analyses of the model weights, we found that the affective intensity and valence were represented in spatially distinct areas even within the same anatomical brain regions. In addition, the two predictive models were correlated with distinct large-scale functional brain networks—i.e., the ventral attention network was correlated with the affective intensity model, whereas the limbic and default mode networks were correlated with the valence model. These findings are in line with previous studies suggesting that the ventral attention network is important for detecting and identifying important and relevant stimuli given

one's current contexts (38, 40, 55), while the limbic and default mode networks are important for modality-general value information (16, 56) and subjective affective values (57–59). Thus, our results suggest that the affective intensity and valence are processed with distinct brain circuits that are colocalized but connected to distinct large-scale brain systems. This can serve as a guiding hypothesis for more invasive animal studies targeting detailed neural pathways.

Finally, we also identified some brain regions only predictive of either pleasure or pain. The pain-predictive brain regions included the anterior midcingulate cortex (mPFC07), which is known to be preferentially associated with pain among many relevant functions such as negative emotion and cognitive control (60). Some lateral PFC regions (IPFC03 and 13) also appeared to be predictive of pain. These regions are part of the frontoparietal network, which is known to be important for pain, particularly chronic and sustained pain (61–63). Except for these lateral prefrontal regions, the pain-predictive regions also showed substantial spatial overlaps with the neurologic pain signature (NPS) (64). The dorsal posterior part of the insular cortex has been implicated for pain processing but was not identified as a pain-predictive region in our results, which is discussed in detail in *SI Appendix, Discussion*. The pleasure-predictive brain regions included the insular and primary gustatory cortex regions, which could reflect that the affective experience was induced by gustatory stimuli (65).

This study also has some limitations. First, although our information mapping and predictive modeling analyses showed significant decoding performances, their effect sizes were small to medium. Although this is not ideal, we reasoned that the small to medium effect sizes are acceptable in our cases. For example, the main goal of region-level information mapping was to identify the brain regions that contain information about pleasure and pain, not to develop predictive models with the highest effect sizes. In addition, the predictive models of affective intensity and valence showed significant prediction performance even in the independent test dataset. Thus, our results demonstrated that the predictive models were robust despite their small to medium effect sizes. Future studies could explore enhancing prediction performance by using large sample sizes and supervised dimension reduction techniques such as partial least squares, given that the regression based on the first few PCs may fail if the dependent variables are strongly correlated to the last few PCs (66). Second, we only used the brain activation patterns for our predictive modeling. Since the experience of sustained pleasure and pain may induce global changes that persist for an extended period of time, an alternative approach could be to utilize patterns of functional connectivity, as we did in our previous study (63). Though we focused on the activation patterns to identify brain regions for pleasure and pain in the current study, we could use both activation and connectivity patterns to maximize the prediction performance. This possibility should be examined in future studies. Third, the brain regions only predictive of either pain or pleasure might also encode salience or other processes, rather than exclusively related to pain or pleasure. However, the primary goal of this study was to identify the brain regions encoding both pain and pleasure information and to dissociate the intensity and valence codes across these regions. To pinpoint brain regions that are more specifically related to each domain, we may need a better control condition that has salience dynamics that are well matched to those in the pain and pleasure conditions. Fourth, the pain and pleasure experiences induced by capsaicin and chocolate stimuli were unbalanced. Although we tried to mitigate potential bias from this imbalance by subsampling ratings, this procedure tended to exclude the time points with high unpleasantness scores within the pain condition

more frequently. This might result in capturing different aspects of sustained pain and pleasure by our modeling. Future research should balance the overall levels of pleasantness and unpleasantness ratings to avoid other potential effects of this subsampling. Fifth, we did not strictly control participants' most recent meals, satiety levels, or baseline taste preferences. Although we found no significant association between participants' (un)pleasantness ratings on capsaicin and chocolate and their sensitivity to relevant tastes (34, 67) (*SI Appendix, Fig. S27*), future studies could aim to control better for these variables. Finally, compared to Study 1, Study 2 exhibited lower pain and pleasure ratings, potentially attributable to variations in experimental conditions (see also *SI Appendix, Discussion*). While our intensity and valence models showed consistent performance across both studies, caution is needed in interpreting these results.

Overall, the current study provides insights into the brain representations of affective valence and intensity across pleasure and pain, promoting the system-level understanding of human affective experiences.

## Materials and Methods

More detailed information can be found in *SI Appendix, Materials and Methods*.

**Ethical Statement.** All participants provided written informed consent. The study protocol was approved by the institutional review board (IRB) of Sungkyunkwan University.

**Region-level Information Mapping.** To identify which brain regions were predictive of pain or pleasure, we conducted predictive modeling based on multivariate patterns of brain activity for different brain regions. We first defined 48 a priori ROIs covering the brainstem, subcortical regions, and prefrontal regions, based on previous studies (35–37) and the Harvard-Oxford brain atlas. For each ROI, we trained predictive models of pain or pleasure using the PCR algorithm. The modeling was based on the concatenated fMRI data across all 34 time-bins, conditions (i.e., capsaicin and control conditions or chocolate and control conditions), and participants. We selected 13 principal components (PCs) to train regression models (please see *SI Appendix, Materials and Methods*, for how we selected 13 PCs) and then transformed the PC regression weights back to the voxel space for each brain region. We also tested different PC numbers for different levels of explained variance (i.e., 65%, 70%, 75%, 80%, and 85%), which showed similar performances with gradual changes (*SI Appendix, Figs. S12 and S13*). The numbers of voxels and explained variances of 48 ROIs across different PC numbers are provided in *SI Appendix, Table S3*.

We evaluated the mean within-individual correlation between predicted and actual outcomes (i.e., pleasantness–unpleasantness ratings) with the LOSO-CV. We examined their statistical significance using bootstrap tests with 10,000 iterations to test whether the bootstrapped distribution of the within-individual correlations significantly deviated from zero. The ROIs that showed statistically significant predictions for both pleasantness and unpleasantness ratings (FDR-corrected) were selected for further analyses of affective intensity and valence. We used the Benjamini-Hochberg procedure for the FDR correction (68).

**Predictive Modeling of Affective Intensity and Valence.** To examine how the seven brain regions for pain and pleasure encode two core affective dimensions—*affective intensity* and *valence*—we first defined *affective intensity* as the absolute values of pleasantness–unpleasantness ratings and *affective valence* as the raw signed values of pleasantness–unpleasantness ratings. Using these as outcomes, we developed the PCR models to predict *affective intensity* and *valence* across all conditions (i.e., capsaicin, chocolate, and control) and participants. We used all the voxels within the seven brain regions for this modeling (please see *SI Appendix, Materials and Methods*, for the details).

The other procedures of predictive modeling were identical to the region-level information mapping. The number of PCs that explained 75% of the total variance was 123 for both intensity and valence models, and thus, we chose to use 123 PCs for the PCR modeling. We obtained the predictive weights of intensity and valence by transforming the PC regression weights back to the voxel space. Prediction

performances of the intensity and valence models were evaluated using LOSO-CV. To examine the robustness of these two models, we also tried 1) developing PCR models to predict the original rating values instead of the ranks and 2) using the whole 48 ROIs (*SI Appendix, Fig. S16*). The procedure of predictive modeling of intensity and valence for each of the seven overlapping brain regions was also identical, using 31 PCs based on the same method used to choose the number of PCs in the region-level information mapping (*SI Appendix, Tables S1 and S2*).

The model predictions (or model responses) were calculated as the dot product of vectorized brain activity with predictive weights, which we termed pattern expression (i.e., the expression of the multivariate pattern of a predictive model).

$$\text{Pattern expression} = \bar{w} \cdot \bar{x} = \sum_{i=1}^n w_i x_i,$$

where  $n$  is the number of voxels,  $w$  is the predictive weights, and  $x$  is the fMRI data. To minimize bias in the estimation of model performance, we used LOSO-CV—i.e., pattern expression values of one participant were calculated using the predictive weights trained on the data after excluding the participant's data. We calculated the prediction-outcome correlation (i.e., a correlation between the pattern expression values and actual outcomes) for each individual and conducted bootstrap tests (i.e., resampling with replacement) on the correlation values with 10,000 iterations. To identify the significant predictive weights, we conducted bootstrap tests with 10,000 iterations using the same PC number (= 123). We then tested whether the bootstrapped distribution of the predictive weights significantly deviated from zero. To test the generalizability of the models, we tested them on an independent test dataset (Study 2) with no ad hoc tuning of the predictive weights. We calculated the prediction-outcome correlation for each participant and conducted bootstrap tests.

**Whole-brain Functional Connectivity Analysis of the Intensity and Valence Models.** To examine which brain regions and networks are correlated with the predictive models of affective intensity and valence, we calculated the correlations between the pattern expression values and the whole-brain fMRI data. We used the data of the control condition of Study 1 for this analysis because it involved no painful or pleasant stimulation and thus reflected the intrinsic brain activity. For each participant, this analysis yielded the whole-brain functional connectivity maps with pattern expression values as seeds (45). We then conducted *t* test to test whether the functional connectivity was significantly greater than zero across participants (i.e., positive connectivity) with FDR correction. We did not consider negative connectivity because anticorrelations were difficult to interpret. However, for completeness, we also obtained the thresholded functional connectivity maps with both positive and negative correlations in *SI Appendix, Fig. S23*. We also calculated how many suprathreshold voxels were included in each large-scale functional brain network (44).

**Data, Materials, and Software Availability.** The data and codes used to generate the main figures, including regions-of-interests, predictive models, and connectivity maps, are shared through Zenodo.org (<https://zenodo.org/records/11239415>) (69). In-house Matlab codes for fMRI data analyses are available at <https://github.com/canlab/CanlabCore> (70) and <https://github.com/cocoanlab/cocoanCORE> (71).

**ACKNOWLEDGMENTS.** This work was supported by IBS-R015-D1 (Institute for Basic Science; to C.-W.W.), 2019R1C1C1004512, 2021M3E5D2A01022515 (National Research Foundation of Korea; C.-W.W.), and 2E30410-20-085 (KIST Institutional Program; C.-W.W.). This work was also supported by a grant of the Korea Health Technology R&D Project through the Korea Health Industry Development Institute (KHIDI), funded by the Ministry of Health & Welfare, Republic of Korea (Grant Number: HI19C1328).

Author affiliations: <sup>a</sup>Center for Neuroscience Imaging Research, Institute for Basic Science, Suwon 16419, Republic of Korea; <sup>b</sup>Department of Biomedical Engineering, Sungkyunkwan University, Suwon 16419, Republic of Korea; <sup>c</sup>Department of Intelligent Precision Healthcare Convergence, Sungkyunkwan University, Suwon 16419, Republic of Korea; <sup>d</sup>Korea Brain Research Institute, Daegu 41062, Republic of Korea; <sup>e</sup>School of Biological Sciences, Seoul National University, Seoul 08826, Republic of Korea; <sup>f</sup>Department of Psychological and Brain Sciences, Dartmouth College, Hanover, NH 03755; and <sup>g</sup>Life-inspired Neural Network for Prediction and Optimization Research Group, Suwon 16419, Republic of Korea

1. J. Bentham, *An Introduction to the Principles of Morals and Legislation* (Dover Publications, 1780), vol. 45, pp. 527.
2. D.-M. Ellingsen, M. L. Kringelbach, S. Leknes, "A neuroscience perspective on pleasure and pain" in *Philosophy of Pain: Unpleasantness, Emotion, and Deviance*, D. Bain, Ed. (Routledge, New York, 2018), p. 1, online resource.
3. C. B. Saper, The central autonomic nervous system: Conscious visceral perception and autonomic pattern generation. *Annu. Rev. Neurosci.* **25**, 433–469 (2002).
4. K. C. Berridge, M. L. Kringelbach, Pleasure systems in the brain. *Neuron* **86**, 646–664 (2015).
5. S. V. Shinkareva et al., Representations of modality-specific affective processing for visual and auditory stimuli derived from functional magnetic resonance imaging data: Modality-specific affective processing. *Hum. Brain Mapping* **35**, 3558–3568 (2014).
6. J. Kim, S. V. Shinkareva, D. H. Wedell, Representations of modality-general valence for videos and music derived from fMRI data. *Neuroimage* **148**, 42–54 (2017).
7. L. F. Barrett, E. Bliss-Moreau, Affect as a psychological primitive. *Adv. Exp. Soc. Psychol.* **41**, 167–218 (2009).
8. T. D. Wager et al., "The neuroimaging of emotion" in *Handbook of Emotions* (The Guilford Press, New York, NY, ed. 3, 2008), pp. 249–271.
9. J. A. Russell, L. F. Barrett, Core affect, prototypical emotional episodes, and other things called emotion: Dissecting the elephant. *J. Pers. Soc. Psychol.* **76**, 805–819 (1999).
10. M. M. Bradley, B. N. Cuthbert, P. J. Lang, Lateralized startle probes in the study of emotion. *Psychophysiology* **33**, 156–161 (1996).
11. S. Schachter, J. E. Singer, Cognitive, social, and physiological determinants of emotional state. *Psychol. Rev.* **69**, 379–399 (1962).
12. P. J. Lang, M. M. Bradley, B. N. Cuthbert, Emotion and motivation: Measuring affective perception. *J. Clin. Neurophysiol.* **15**, 397–408 (1998).
13. S. Leknes, I. Tracey, A common neurobiology for pain and pleasure. *Nat. Rev. Neurosci.* **9**, 314–320 (2008).
14. K. C. Berridge, T. E. Robinson, Parsing reward. *Trends Neurosci.* **26**, 507–513 (2003).
15. E. Navratilova, C. W. Atcherley, F. Porreca, Brain circuits encoding reward from pain relief. *Trend Neurosci.* **38**, 741–750 (2015).
16. J. Chikazoe, D. H. Lee, N. Kriegeskorte, A. K. Anderson, Population coding of affect across stimuli, modalities and individuals. *Nat. Neurosci.* **17**, 1114–1122 (2014).
17. F. Grabenhorst, E. T. Rolls, C. Margot, M. A. A. P. da Silva, M. I. Velazco, How pleasant and unpleasant stimuli combine in different brain regions: Odor mixtures. *J. Neurosci.* **27**, 13532–13540 (2007).
18. H. Iwaoiki, K. Nakamura, Neuronal encoding of emotional valence and intensity in the monkey amygdala. *J. Neurosci.* **42**, 7615–7623 (2022).
19. J. J. Paton, M. A. Belova, S. E. Morrison, C. D. Salzman, The primate amygdala represents the positive and negative value of visual stimuli during learning. *Nature* **439**, 865–870 (2006).
20. G. Corder et al., An amygdala neural ensemble that encodes the unpleasantness of pain. *Science* **363**, 276–281 (2019).
21. J.-S. Lu, Q.-Y. Chen, S. Zhou, K. Inokuchi, M. Zhuo, Dual roles of anterior cingulate cortex neurons in pain and pleasure in adult mice. *Mol. Brain* **11**, 72 (2018).
22. K. C. Berridge, Affective valence in the brain: Modules or modes? *Nat. Rev. Neurosci.* **20**, 225–234 (2019).
23. K. A. Lindquist, A. B. Satpute, T. D. Wager, J. Weber, L. F. Barrett, The brain basis of positive and negative affect: Evidence from a meta-analysis of the human neuroimaging literature. *Cereb. Cortex* **26**, 1910–1922 (2016).
24. J. Kim et al., A study in affect: Predicting valence from fMRI data. *Neuropsychologia* **143**, 107473 (2020).
25. S. J. Shabel, P. H. Janak, Substantial similarity in amygdala neuronal activity during conditioned appetitive and aversive emotional arousal. *Proc. Natl. Acad. Sci. U.S.A.* **106**, 15031–15036 (2009).
26. T. Kahnt, S. O. Park, J. D. Haynes, P. N. Tobler, Disentangling neural representations of value and salience in the human brain. *Proc. Natl. Acad. Sci. U.S.A.* **111**, 5000–5005 (2014).
27. C. Yan et al., Multivariate neural representations of value during reward anticipation and consummation in the human orbitofrontal cortex. *Sci. Rep.* **6**, 29079 (2016).
28. K. A. Lindquist, T. D. Wager, H. Kober, E. Bliss-Moreau, L. F. Barrett, The brain basis of emotion: A meta-analytic review. *Behav. Brain Sci.* **35**, 121–143 (2012).
29. C. D. Wilson-Mendenhall, L. F. Barrett, L. W. Barsalou, Neural evidence that human emotions share core affective properties. *Psychol. Sci.* **24**, 947–956 (2013).
30. N. Kriegeskorte, R. Goebel, P. Bandettini, Information-based functional brain mapping. *Proc. Natl. Acad. Sci. U.S.A.* **103**, 3863–3868 (2006).
31. C.-W. Woo, L. J. Chang, M. A. Lindquist, T. D. Wager, Building better biomarkers: Brain models in translational neuroimaging. *Nat. Neurosci.* **20**, 365–377 (2017).
32. M. Roy et al., Representation of aversive prediction errors in the human periaqueductal gray. *Nat. Neurosci.* **17**, 1607–1612 (2014).
33. B. Horing, C. Sprenger, C. Buchel, The parietal operculum preferentially encodes heat pain and not salience. *PLoS Biol.* **17**, e3000205 (2019).
34. L. M. Bartoshuk et al., Valid across-group comparisons with labeled scales: The gLMS versus magnitude matching. *Physiol. Behav.* **82**, 109–114 (2004).
35. T. E. Kravnak, A. L. Marsland, T. D. Wager, P. J. Gianaros, Functional neuroanatomy of peripheral inflammatory physiology: A meta-analysis of human neuroimaging studies. *Neurosci. Biobehav. Rev.* **94**, 76–92 (2018).
36. I. Faillenot, R. A. Heckemann, M. Frot, A. Hammers, Macroanatomy and 3D probabilistic atlas of the human insula. *NeuroImage* **150**, 88–98 (2017).
37. A. de la Vega, L. J. Chang, M. T. Banich, T. D. Wager, T. Yarkoni, Large-scale meta-analysis of human medial frontal cortex reveals tripartite functional organization. *J. Neurosci.* **36**, 6553–6562 (2016).
38. E. T. Rolls, Functions of the anterior insula in taste, autonomic, and related functions. *Brain Cogn.* **110**, 4–19 (2016).
39. W. W. Seeley, The salience network: A neural system for perceiving and responding to homeostatic demands. *J. Neurosci.* **39**, 9878–9882 (2019).
40. V. Menon, L. Q. Uddin, Salient, switching, attention and control: A network model of insula function. *Brain Struct. Function* **214**, 655–667 (2010).
41. K. M. Tye et al., Amygdala circuitry mediating reversible and bidirectional control of anxiety. *Nature* **471**, 358–362 (2011).
42. L. Wang et al., The coding of valence and identity in the mammalian taste system. *Nature* **558**, 127–131 (2018).
43. L. E. Simons et al., The human amygdala and pain: Evidence from neuroimaging. *Hum. Brain Mapp.* **35**, 527–538 (2014).
44. B. T. Yeo et al., The organization of the human cerebral cortex estimated by intrinsic functional connectivity. *J. Neurophysiol.* **106**, 1125–1165 (2011).
45. C.-W. Woo et al., Separate neural representations for physical pain and social rejection. *Nat. Commun.* **5**, 5380 (2014).
46. M. Čeko, P. A. Kragel, C.-W. Woo, M. López-Solà, T. D. Wager, Common and stimulus-type-specific brain representations of negative affect. *Nat. Neurosci.* **25**, 760–770 (2022).
47. S. Freud, *Sigmund Freud Collection (Library of Congress), Beyond the Pleasure Principle, The International Psycho-analytical Library* (Liveright, New York, 1950), pp. 97.
48. A. B. Fernando, J. E. Murray, A. L. Milton, The amygdala: Securing pleasure and avoiding pain. *Front. Behav. Neurosci.* **7**, 190 (2013).
49. S. Leknes et al., The importance of context: When relative relief renders pain pleasant. *Pain* **154**, 402–410 (2013).
50. S. Leknes, M. Lee, C. Berna, J. Andersson, I. Tracey, Relief as a reward: Hedonic and neural responses to safety from pain. *PLoS One* **6**, e17870 (2011).
51. D. M. Ellingsen et al., Placebo improves pleasure and pain through opposite modulation of sensory processing. *Proc. Natl. Acad. Sci. U.S.A.* **110**, 17993–17998 (2013).
52. H. L. Fields, How expectations influence pain. *Pain* **159** (suppl. 1), S3–S10 (2018).
53. T. D. Wager, L. Y. Atlas, The neuroscience of placebo effects: Connecting context, learning and health. *Nat. Rev. Neurosci.* **16**, 403–418 (2015).
54. S. Becker et al., The role of hedonics in the Human Affectome. *Neurosci. Biobehav. Rev.* **102**, 221–241 (2019).
55. M. Corbetta, G. Patel, G. L. Shulman, The reorienting system of the human brain: From environment to theory of mind. *Neuron* **58**, 306–324 (2008).
56. D. McNamee, A. Rangel, J. P. O'Doherty, Category-dependent and category-independent goal-value codes in human ventromedial prefrontal cortex. *Nat. Neurosci.* **16**, 479–485 (2013).
57. L. Koban, P. J. Gianaros, H. Kober, T. D. Wager, The self in context: Brain systems linking mental and physical health. *Nat. Rev. Neurosci.* **22**, 309–322 (2021).
58. F. Grabenhorst, E. T. Rolls, Value, pleasure and choice in the ventral prefrontal cortex. *Trends Cogn. Sci.* **15**, 56–67 (2011).
59. O. Bartra, J. T. McGuire, J. W. Kable, The valuation system: A coordinate-based meta-analysis of BOLD fMRI experiments examining neural correlates of subjective value. *NeuroImage* **76**, 412–427 (2013).
60. P. A. Kragel et al., Generalizable representations of pain, cognitive control, and negative emotion in medial frontal cortex. *Nat. Neurosci.* **21**, 283–289 (2018).
61. A. Kucyi, T. V. Salomons, K. D. Davis, Cognitive behavioral training reverses the effect of pain exposure on brain network activity. *Pain* **157**, 1895–1904 (2016).
62. D. A. Seminowicz, M. Moayedi, The dorsolateral prefrontal cortex in acute and chronic pain. *J. Pain* **18**, 1027–1035 (2017).
63. J. J. Lee et al., A neuroimaging biomarker for sustained experimental and clinical pain. *Nat. Med.* **27**, 174–182 (2021).
64. T. D. Wager et al., An fMRI-based neurologic signature of physical pain. *N. Engl. J. Med.* **368**, 1388–1397 (2013).
65. A. B. Satpute et al., Involvement of sensory regions in affective experience: A meta-analysis. *Front. Psychol.* **6**, 1860 (2015).
66. A. S. Hadi, R. F. Ling, Some cautionary notes on the use of principal components regression. *Am. Stat.* **52**, 15–19 (1998).
67. L. E. Marks et al., Magnitude-matching: The measurement of taste and smell. *Chem. Senses* **13**, 63–87 (1988).
68. Y. Benjamini, Y. Hochberg, Controlling the false discovery rate: A practical and powerful approach to multiple testing. *J. R. Statist. Soc. Ser. B Methodol.* **57**, 289–300 (1995).
69. S. A. Lee et al., Brain representations of affective valence and intensity in sustained pleasure and pain. Zenodo. <https://zenodo.org/records/11239415>. Deposited 23 May 2024.
70. T. D. Wager, (Cognitive and Affective Neuroscience Lab) CanlabCore, Github. <https://github.com/canlab/CanlabCore>. Accessed 1 September 2019.
71. C.-W. Woo, (Computational Cognitive Affective Neuroscience Lab) cocoanCORE, Github. <https://github.com/cocoanlab/cocoanCORE>. Accessed 1 March 2020.